

# Superficial segregation, wetting, and dynamical equilibrium in bimetallic clusters: A Monte Carlo study

F. Lequien, J. Creuze,\* F. Berthier, and I. Braems  
*LEMHE/ICMMO, Bâtiment 410, Université Paris Sud-XI, F91405 Orsay Cedex, France*

B. Legrand  
*SRMP-DMN, CEA Saclay, F91191 Gif-sur-Yvette Cedex, France*

(Received 31 March 2008; revised manuscript received 10 July 2008; published 12 August 2008)

Using Monte Carlo simulations on a lattice-gas model within the pseudo-grand-canonical ensemble, we study the competition between superficial segregation, wetting and a core dynamical equilibrium for nanoparticles made of thousands of atoms in a system that tends to phase separate, e.g., Cu-Ag. Increasing the chemical potential difference  $\Delta\mu$  between Ag and Cu (or the nominal Ag concentration) at a temperature lower than the critical temperature for the phase separation in the infinite crystal, we show that the cluster goes through different stages: (i) Ag-superficial segregation that involves the vertices first, then the edges, and finally the (111) and (001) facets; (ii) prewetting that leads to Ag enrichment on the shells close to the cluster surface; (iii) a dynamical equilibrium that affects all the internal shells jointly, similar to the first-order phase transition due to the miscibility gap in an infinite crystal; and (iv) again standard segregation. Moreover, we show that a similar behavior occurs for the cluster facets if the temperature is lower than the critical temperatures of the first-order phase transition of the corresponding surfaces of semi-infinite crystals. A remarkable consequence of those dynamical equilibria is that very different concentrations of the facets on one hand and of the whole cluster on the other hand can be observed at a given  $\Delta\mu$ .

DOI: [10.1103/PhysRevB.78.075414](https://doi.org/10.1103/PhysRevB.78.075414)

PACS number(s): 64.75.Jk, 68.35.Rh

## I. INTRODUCTION

Multiconstituent nanostructures have recently attracted much attention, from both the experimental and theoretical points of view, since it is possible to obtain dramatic changes in chemical,<sup>1-5</sup> magnetic,<sup>6,7</sup> and optical properties<sup>8-10</sup> compared to those of the individual metals. Indeed, bimetallic clusters represent a large family of constructors where both the size and the chemical composition play a significant role in their structures and thus in their chemical and physical properties. The order and phase stability in bulk alloys<sup>11</sup> together with superficial segregation in alloy surfaces<sup>12</sup> have been intensively studied over the last 20 years. The same issues are now investigated concerning finite-size systems,<sup>13-19</sup> the structure and chemical ordering of bimetallic clusters having given rise already to many experimental and theoretical studies over the last 10 years.<sup>20,21</sup>

To specify the finite-size effect on superficial segregation, the comparison of the segregation isotherms in semi-infinite alloys and in the outermost shells of clusters is an interesting tool. Hence, a recent study showed that the anisotropy of the superficial segregation between the (111) and the (001) facets of the cuboctahedron could strongly differ from the segregation anisotropy predicted between the (111) and the (001) surfaces of semi-infinite alloys.<sup>13</sup> More precisely, computations relying on an Ising model fitted for the Cu-Ag system revealed that while the usual anisotropy of semi-infinite surfaces, corresponding to a more important enrichment of the more open surface [here the (001) surface versus the (111) one], is established for clusters of at least  $10^5$  atoms, for smaller clusters the (111) facets are more Ag enriched than the (001) facets. If the anisotropy of superficial segregation varies with the cluster size, what happens to the superficial

phase transitions that occur in phase-separating systems such as Cu-Ag? In semi-infinite alloys, the surfaces of such systems display segregation isotherms of the Fowler-Guggenheim type.<sup>12,22</sup> They are characterized by the existence of a critical temperature below which the segregation isotherm undergoes a first-order phase transition that corresponds to a jump in the superficial concentration for a critical bulk concentration or equivalently for a critical difference of chemical potentials between both metals.<sup>12</sup> At room temperature, in the Cu(Ag) system, the infinite surface shifts from an almost Cu-pure state to an almost Ag-pure state for a very low Ag bulk concentration (less than 0.1%).<sup>23-27</sup> Moreover, for alloys where a bulk order-disorder transition exists, it is known that a wetting by the disordered phase can occur at temperatures lower than the bulk critical one.<sup>28</sup> For alloys with a tendency to bulk phase separation, this wetting phenomenon manifests itself by the occurrence of an infinite number of two-dimensional (2D) phase-separation transitions, affecting successively each layer parallel to the surface, when approaching the critical temperature at fixed bulk concentration.<sup>29,30</sup>

This work aims at studying the evolution of such phenomena (phase transition and wetting) when one switches from infinite or semi-infinite alloys to nanoparticles. We therefore consider the same lattice-gas model with pair interactions as mentioned here above, and we specify in Sec. II its extension to the cuboctahedron case and how the main parameters have been fitted to the Cu-Ag system. In Sec. III, we present the segregation isotherms obtained by Monte Carlo simulations at 300 K and analyze in detail both the mean concentrations of the (001) facets and the concentration fluctuations of each facet during the Monte Carlo simulations. We then study in Sec. IV the nanoparticle behavior on the whole range of the

Ag nominal concentration at two temperatures (below and above the bulk critical temperature of phase-separation transition). As a result, we emphasize the existence of a dynamical equilibrium, both at the surface and in the core of the cluster. The first one corresponds to the extension of the first-order phase transitions of infinite surfaces to facets, while the second one corresponds to the equivalent of a bulk phase separation in an infinite crystal. In Sec. V, we discuss the main question arising, i.e., how the behavior of a semi-infinite system is recovered, and we draw our conclusions in Sec. VI.

## II. MODELS

To benefit from the previous study of the segregation isotherms in nanoalloys within a mean-field framework,<sup>13</sup> we consider the same Ising model which is governed by two parameters in the superficial segregation context:  $\tau = \frac{1}{2}(V_{AA} - V_{BB})$  and  $V = \frac{1}{2}(V_{AA} + V_{BB} - 2V_{AB})$ , where  $V_{AA}$ ,  $V_{BB}$ , and  $V_{AB}$  are the nearest-neighbor pair interactions between  $A$ - $A$ ,  $B$ - $B$ , and  $A$ - $B$  atoms. The main features of the Cu-Ag system are reproduced by ascribing  $\tau = \frac{1}{2}(V_{AgAg} - V_{CuCu}) = \frac{1}{Z}(E_{coh}^{Ag} - E_{coh}^{Cu}) = 46$  meV and  $V = -\frac{1}{Z}\Delta H_{dis} = -30$  meV,<sup>13</sup> where  $\Delta H_{dis}$  is the enthalpy of mixing in the Cu(Ag) solid solution and  $Z$  is the nearest-neighbor coordination number of the infinite crystal.  $\tau$  is positive due to the lower cohesion energy of Ag as regards to that of Cu, leading to Ag segregation on less coordinated sites,<sup>12</sup> even if the difference in surface energies,  $\Delta\gamma^{hkl} = \Delta Z^{hkl}\tau$ , where  $\Delta Z^{hkl}$  is the number of broken bonds of an  $(hkl)$  surface, is slightly overestimated when compared with *ab initio* calculations or simulations employing  $N$ -body-type interatomic potentials. The tendency to phase separate of the Cu-Ag alloy is ensured by the negative value of  $V$ , leading to the existence of critical temperatures for both the bulk and the surfaces,<sup>12</sup> even if the asymmetry of the Cu-Ag bulk phase diagram is lost when neglecting the dependence of  $V$  on the concentration. In the mean-field approximation and for a monolayer model of the (111) and (001) surfaces,<sup>31</sup> these critical temperatures are given by  $k_B T_c^{bulk} = -6V$ ,  $k_B T_c^{(111)} = -3V$ , and  $k_B T_c^{(001)} = -2V$ , i.e.,  $T_c^{bulk} = 2088$  K,  $T_c^{(111)} = 1044$  K, and  $T_c^{(001)} = 696$  K. Recall that the mean-field approximation overestimates the critical temperatures by a crystallographic ratio:<sup>11</sup> 1.22 for the bulk and 1.64 and 1.76 for the (111) and (001) surfaces, respectively.<sup>32</sup> The exact critical temperatures (obtained by Monte Carlo simulations, for instance) are then equal to 1711 K for the bulk, 637 and 395 K for the (111) and (001) infinite surfaces, respectively. Note that this rigid-lattice approach can be extended to take into account atomic relaxations partially by considering effective values for the energetic parameters obtained via  $N$ -body interatomic potentials, as demonstrated in the case of grain boundaries and reconstructed surfaces in the Cu-Ag system.<sup>33–35</sup>

We study the 3871-atom cuboctahedron, whose outermost shell can be described as follows: adding to 12 vertices of coordination 5 and 24 edges of coordination 7, it owns 6 square (001) facets of coordination 8 and 8 triangular facets (111) of coordination 9. Moreover, the cuboctahedral cluster is made of a successive packing of atoms as follows: the

central atom surrounded by its 12 nearest neighbors of the fcc structure defines the nanoparticle of order  $n=1$ . Adding a new shell of nearest neighbors gives the nanoparticle of order  $n=2$  and so on. The 3871-atom nanoparticle corresponds to  $n=10$ , each shell being denoted  $S_i$  in the following (from  $i=1$  for the outermost shell up to  $i=10$  for the central site and its 12 nearest neighbors). Note that this size is well beyond the critical size that separates the stability domains of the icosahedron from structures issued from the fcc lattice (cuboctahedron and especially the truncated octahedron), even if decahedral structures are highly competitive up to  $10^4$  atoms for Cu and Ag clusters.<sup>36,37</sup>

To determine the distribution of Cu and Ag atoms onto the different sites of the cluster, we perform Monte Carlo simulations in the pseudo-grand-canonical ensemble,<sup>38,39</sup> where the nominal concentration of the  $Ag_c Cu_{1-c}$  cluster is determined by the chemical potential difference  $\Delta\mu = \mu_{Ag} - \mu_{Cu}$ . Similar to the studies of massive alloys, the choice of the pseudo-grand-canonical ensemble instead of the canonical one (where the nominal concentration is imposed by the relative proportion of Ag and Cu atoms initially introduced) allows one to obtain a better description of the phase transition characteristics.<sup>11</sup> We shall discuss later on the comparison with experiments, which are closer to a canonical-ensemble study. A standard Metropolis algorithm is used<sup>39,40</sup> and the averages are evaluated over  $2 \times 10^5$  Monte Carlo (MC) macrosteps, a similar number of macrosteps used to reach equilibrium. A MC macrostep corresponds to  $N_{at}$  propositions of chemical switch,  $N_{at}$  being the total number of atoms of the cluster. This allows us to obtain the mean concentrations on the different sites by accounting for short-range order, contrary to the mean-field framework.

## III. SUPERFICIAL SEGREGATION IN BIMETALLIC CLUSTERS

Segregation isotherms for the sites in the vertices, edges, and (001) and (111) facets obtained at  $T=300$  K by Monte Carlo simulations are shown in Fig. 1. Note that for the values of  $\Delta\mu$  we consider here, only the surface is enriched in Ag, the underlying layers and the core of the cluster remaining almost Cu pure.<sup>13</sup> Due to the lowest coordination number of the vertices, the relative isotherm is shifted toward the lowest values of  $\Delta\mu$ . Increasing  $\Delta\mu$  leads to a Ag enrichment on the edges, then on the (111) facets, and finally on the (001) facets. Note that the relative position of the isotherms for the two types of facets does not follow the order of increasing coordination numbers. A previous mean-field approach<sup>13</sup> shows that this is due to the coupling with the edges, the classical hierarchy being recovered for clusters with more than 16 shells (12 431 atoms). Comparison between Monte Carlo simulations and mean-field approach shows that the relative positions of the isotherms are in good agreement.<sup>13</sup> Moreover, the mean-field model predicts the existence of a first-order transition for the edges and facets isotherms,<sup>13</sup> whereas Monte Carlo simulations lead to continuous isotherms for any kind of sites. Nevertheless, if the facet isotherms are continuous, they display very stiff variations for a  $\Delta\mu$  range close to the critical values  $\Delta\mu_c$  derived

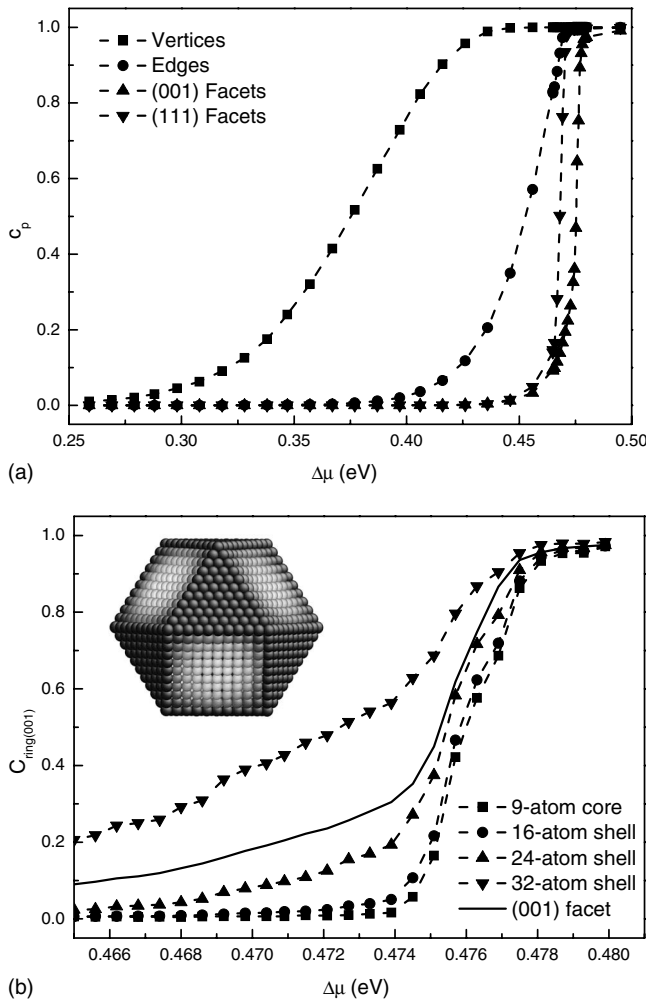


FIG. 1. Segregation isotherms obtained by MC simulations at  $T=300$  K. The concentrations for the different sites of the surface are given as a function of the difference in chemical potentials  $\Delta\mu$  (in eV) (a). Segregation isotherms at  $T=300$  K for the various concentric shells of the (001) facets (b). The isotherm for the facet itself is given by the solid line. The inset presents the equilibrium concentration for each atomic site obtained by MC simulations at  $T=300$  K and  $\Delta\mu=474$  meV. The gray levels vary between white ( $c_p=0$ , Cu pure) and black ( $c_p=1$ , Ag pure).

from the mean-field framework [463 meV for the (111) facets and 474 meV for the (001) facets]. We verified that these isotherms are perfectly reversible, the same curves being obtained by progressively increasing or decreasing  $\Delta\mu$ .

The relative positions of the edges and facets isotherms indicate that the edges are Ag enriched before the segregation phenomenon reaches the facets. As Monte Carlo simulations account for short-range order, contrary to the Bragg-Williams mean-field formalism, we can wonder whether the sites of the facet that are close to the edges are more enriched than the center of the facets. The inset of Fig. 1(b), which shows the equilibrium concentration for each site of the cluster surface at  $\Delta\mu=474$  meV [value of  $\Delta\mu$  for which vertices, edges, and (111) facets are Ag pure, while the mean concentration of the (001) facets equals 0.32], reveals an important inhomogeneity inside the (001) facets: By analyzing the facet as a sequence of concentric square rings (the

central atom, then the rings made of, respectively, 8, 16, 24, and 32 atoms), one observes that the two outermost rings (32- and 24-atom rings) are Ag enriched when compared with the centermost ones. A more detailed analysis shows that the outer concentric rings are also inhomogeneous, the segregation being stronger on the vertices than on the middle of each edge.

Figure 1(b) depicts the variation in the concentration of the concentric square rings of the (001) facets as a function of  $\Delta\mu$ . We gathered the central atom with the innermost eight-atom ring and we display the concentration of these nine central sites, the one of the following three rings, and the mean concentration of the facet [already depicted in Fig. 1(a) but here rescaled in  $\Delta\mu$ ]. This figure shows three regimes for the segregation isotherm of the (001) facets. In the first regime ( $\Delta\mu \leq 474$  meV), the concentration of the two outer rings increases regularly, while the two center rings remain almost Cu pure. This yields the heterogeneity of the facet displayed in the inset of Fig. 1(b). In the second regime ( $474 \text{ meV} \leq \Delta\mu \leq 477 \text{ meV}$ ), the concentrations of all rings increase very rapidly and simultaneously. This last point allows us to exclude a mechanism of progressive Ag enrichment of the facet from the outer rings that would be analogous to the one observed in regime 1. This regime is responsible for the stiff increase in the isotherm associated with the mean concentration of the (001) facets that we shall detail later on. Finally, for  $\Delta\mu \geq 477$  meV, the isotherms reach the saturation and the (001) facets are homogeneous and Ag pure. Note that in the three regimes there is no symmetry break between the facets: The concentration remains the same for all the equivalent sites from a facet to the other as depicted in the inset of Fig. 1(b).

To detail the nature of regime 2 for the (001) facets, which occurs in a very narrow range of  $\Delta\mu$  close to the mean-field critical value  $\Delta\mu_c$  of first-order phase transition between 2D phase separation and disorder, we display in Fig. 2 two snapshots of the cluster surface for  $\Delta\mu=476$  meV. In a same snapshot, the various (001) facets have very different concentrations from each other: Some are almost Ag pure (like regime 3), while the others are very similar to those observed in regime 1 (Ag-enriched outer rings and almost Cu-pure inner rings). Moreover, from one snapshot to the other, the concentration of a same facet can evolve strongly from an almost Ag-pure configuration to a regime 1-type configuration. Thus, each facet undergoes a dynamical equilibrium independently between these two states. This bistability, which characterizes regime 2, is associated with the bimodality of the configurational densities of states (CDOS) shown in Fig. 3. These CDOSs are defined as the number of times the concentration of the innermost ring of a given facet (here defined by the central site and its first 2D ring of nearest neighbors) is between  $c$  and  $c+dc$  during a MC simulation, the densities being normalized to 1. In regimes 1 and 3, the CDOS is unimodal, whereas it becomes bimodal in regime 2. Therefore, the sharp rise in the isotherm in regime 2 corresponds to an increasing (decreasing) occupancy of the almost Ag-pure state ( $c_{(001)F} \approx 1$ ) [almost Cu-pure state ( $c_{(001)F} \approx 0$ )]. Moreover, we note that: (i) the concentrations associated with these two states ( $c_{(001)F} \approx 0.01$  and  $c_{(001)F} \approx 0.97$ ) remain almost constant in the whole regime 2, as this

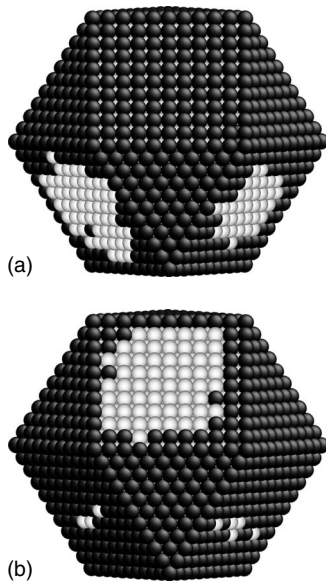


FIG. 2. Two snapshots obtained by Monte Carlo simulations at  $T=300$  K for  $\Delta\mu=476$  meV (regime 2). The white (black) spheres correspond to the Cu (Ag) atoms.

is the case for the solubility limits in an infinite phase-separated system;<sup>11,41</sup> and (ii) the dynamical equilibrium vanishes at high temperature, similar to the corresponding semi-infinite system at a temperature higher than the critical temperature of first-order phase transition between phase separation and disorder. As a consequence, the resulting CDOS becomes unimodal on the whole range of Ag nominal concentration.

Finally, note that the behaviors of the (111) and (001) facets are similar: The three regimes can be observed, with a progressive Ag enrichment from the outer ring in regime 1, a stiff and simultaneous increase in the isotherms in regime 2, and the saturation in regime 3.

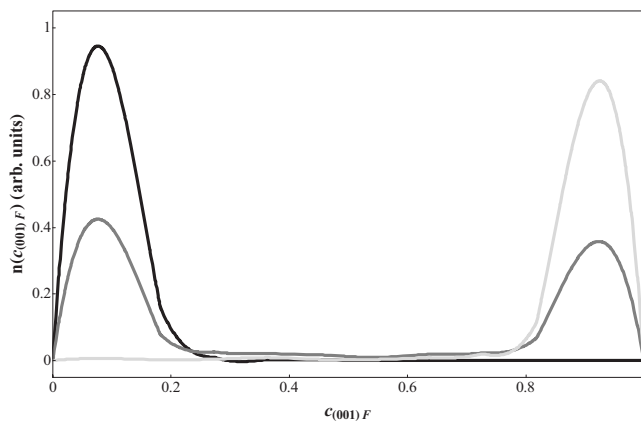


FIG. 3. CDOSs for the central ring (nine sites) of a given (001) facet obtained by MC simulations at  $T=300$  K for  $\Delta\mu=473.2$  meV (regime 1, dark gray),  $\Delta\mu=476$  meV (regime 2, gray), and  $\Delta\mu=480$  meV (light gray). Note that for the sake of clarity, we have drawn the line graphs of the histograms.

#### IV. FROM THE SHELL TO THE CORE

The detailed study of the cluster facets underlines a competition between the two following phenomena: (a) wetting, which can be described as the growth from the edges of a Ag-rich zone due to segregation; and (b) dynamical equilibrium that initiates at the center of the facets, characterized by large fluctuations of the overall facet concentrations between a Cu-rich state and a Ag-rich one. This dynamical equilibrium occurring in finite-size systems is the analog of the first-order phase transitions affecting the surfaces of Cu(Ag) semi-infinite alloys.<sup>12</sup>

In this section, we present the behavior of the internal shells on the whole range of Ag nominal concentration. As for the facets' behavior, characterized by the competition between wetting from the edges and dynamical equilibrium of the facets' center, this will allow us to study the behavior of the whole nanoparticle and thus the possible competition between wetting from the outermost shell (enriched in Ag due to superficial segregation) and core dynamical equilibrium in bimetallic clusters.

##### A. High-temperature limit: $T \gg T_c^{\text{bulk}}$

We first present the high-temperature behavior for which only superficial segregation occurs. Thereby, the temperature is fixed at  $T=3000$  K, well above the bulk critical temperature of phase separation–disorder transition ( $T_c^{\text{bulk}}=1711$  K). Note that if it seems to be a very high temperature, especially if compared with the melting temperatures of copper ( $T_m=1356$  K) and of silver ( $T_m=1233$  K),<sup>42</sup> the variation in the melting temperature of nanoparticles containing impurity atoms can strongly differ from the bulk behavior.<sup>43</sup> Hence, this choice is justified essentially by a methodological aspect. It allows one to study the cluster behavior in the solid solution over the whole concentration range. This is feasible within a rigid-lattice approach since it is naturally free from melting phenomenon.

Figure 4(a) shows the concentration of the different cluster shells as a function of  $\Delta\mu$  as well as the core one, the core being constituted by the 55 central sites, i.e., the central site ( $S_{11}$  shell) with its 12 nearest neighbors ( $S_{10}$  shell) and the 42 sites of the  $S_9$  shell. Joining these sites on which the concentration is almost homogeneous enables one to obtain a good statistics in the core region. At this temperature, only the superficial concentration differs noticeably from the concentration of the other shells, the first underlying shell having an isotherm almost identical to the core one. To enlight the Ag-superficial enrichment, we show in Fig. 4(b) the shell concentrations as a function of the core one, the isotherms' deviation with respect to the bisector being a feature of the superficial segregation over the whole concentration range.

Splitting each concentric shell into its different kinds of sites [ $V$ ,  $E$ ,  $(001)F$ , and  $(111)F$ ], as done for the surface shell (see Sec. III), shows that the segregation hierarchy is still effective on the first underlying shell, even if the effect is very weak at this high temperature. Moreover, the concentration profiles, which represent the shell concentrations  $c_p$  as a function of  $p$ , exhibit a classical exponential decay whatever  $\Delta\mu$  is, as predicted by the mean-field formalism in the

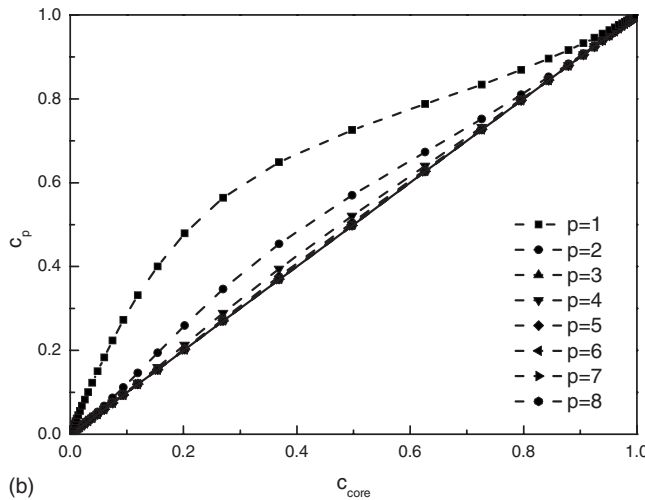
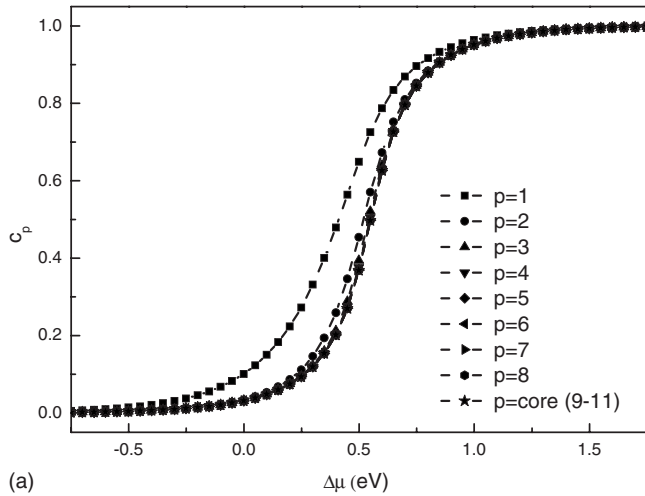


FIG. 4. Concentric shell isotherms,  $c_p=f(\Delta\mu)$  (a) and  $c_p=f(c_{\text{core}})$  (b), obtained by MC simulations at  $T=3000$  K.

disordered state.<sup>44</sup> The corresponding CDOSs are unimodal for all the shells, including the core, which indicates that no dynamical equilibrium occurs, as expected at this high temperature.

**B. Low temperature:  $T \approx 0.887T_c^{\text{bulk}}$**

At a temperature lower than the critical temperature for the phase separation–disorder transition of an infinite crystal, we shall study the evolution of superficial segregation that affects the surface-cluster shell at the vicinity of a bulklike miscibility gap. The latter will be characterized in the following. Figure 5(a) shows the concentrations of the different cluster shells as a function of  $\Delta\mu$  at  $T=1500$  K. In comparison with the previous results obtained at  $T=3000$  K, these isotherms have the following differences:

(a) They are steeper [note the change in the  $\Delta\mu$  scale between Figs. 4(a) and 5(a)] and the differences between the different kinds of sites are more important, at least up to shell 4.

(b) Except for the surface isotherm, all the others exhibit a rather vertical part located at the same value of  $\Delta\mu$

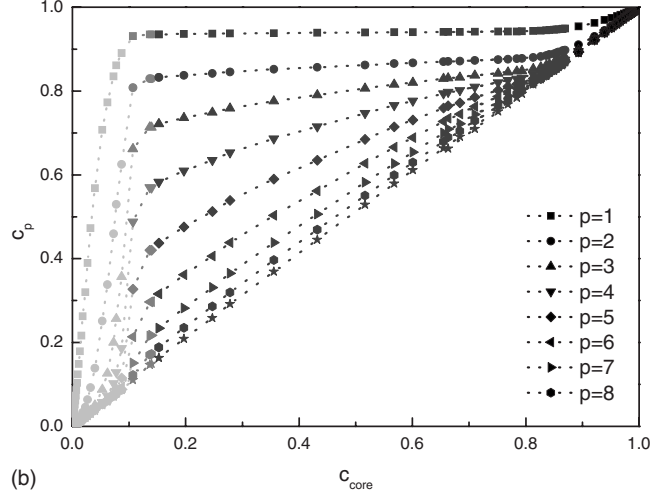
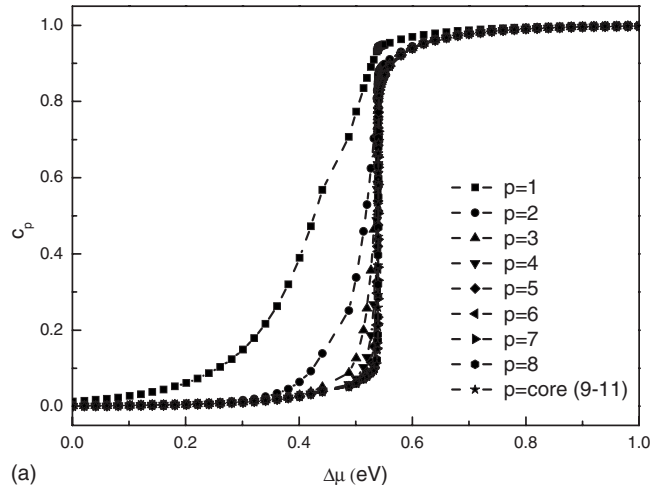


FIG. 5. Concentric shell isotherms,  $c_p=f(\Delta\mu)$  (a) and  $c_p=f(c_{\text{core}})$  (b), obtained by MC simulations at  $T \approx 0.887T_c^{\text{bulk}}$ . The gray levels indicate the domains of existence of each stage of the cluster behavior as a function of  $\Delta\mu$  (or similarly  $c_{\text{core}}$ ).

( $\approx 540$  meV), slightly below the critical value on an infinite bulk ( $\Delta\mu_c^\infty=552$  meV). For the central shells, this part lies between  $c_{\text{central}} \approx 0.15$  and  $c_{\text{central}} \approx 0.85$ . For the intermediate shells (typically from  $c_6$  to  $c_2$ ), the lower bound increases gradually from 0.15 to 0.8 when approaching the cluster surface, while the upper bound varies weakly from 0.85 to 0.9.

(c) Just before this rather vertical part of the isotherms, there is a range of  $\Delta\mu$  (going from 520 to 540 meV) in which some concentrations vary strongly. This mainly concerns shells 3 and 4, the effect being still noticeable for shells 2, 5, and 6.

If we look now at the evolution of the concentrations of the different cluster shells as a function of the core one [Fig. 5(b)], we can divide the cluster behavior into four stages.

**1. Stage I:  $\Delta\mu < 520$  meV or  $c_{\text{core}} < 0.10$**

It is the stage of classical superficial segregation. Silver-superficial segregation increases regularly as  $\Delta\mu$  increases and it mainly affects the first three shells. In the outermost shell, the coupling between the facets and the edges is

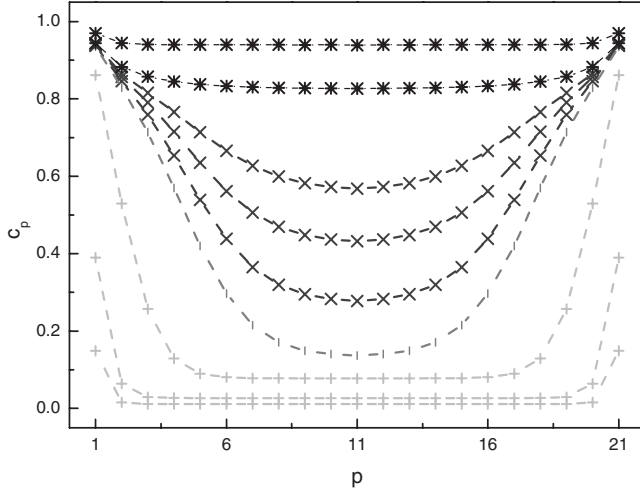


FIG. 6. Concentration profiles,  $c_p = f(p)$ , obtained by MC simulations for various  $\Delta\mu$  at  $T \approx 0.887 T_c^{\text{bulk}}$ . To enhance the finite-size aspect, these profiles are shown along a diameter of the nanoparticle:  $p=1$  and  $p=21$  corresponds to the outermost shell,  $p=2$  and  $p=20$  to the first underlying shell, and so on up to  $p=11$ , which corresponds to the central site. The gray levels indicate the domains of existence of each stage of the cluster behavior as a function of  $\Delta\mu$ , from stage 1 (the lightest) to stage 4 (the darkest).

weaker than for  $T=300$  K, since the cluster surface is in the disordered state, and the classical hierarchy of Ag segregation is recovered; i.e., the relative positions of the isotherms follow the order of increasing coordination numbers  $V/E/(001)F/(111)F$ .<sup>14</sup> Moreover, the same hierarchy is observed for the underlying shells affected by the segregation, due to the couplings with the uppermost shells. The concentration profiles relative to this stage, shown in Fig. 6, still follow an exponential decay but with very small values of the attenuation length, defined here as  $\xi = -[\ln(\delta c_p / \delta c_{p-1})]^{-1}$ , with  $\delta c_p = c_p - c_{\text{core}}$ , and expressed in units of the intershell distance. Note that this prevents the existence of a pure core/shell structure at this temperature.<sup>45</sup>

### 2. Stage II: $520 \text{ meV} < \Delta\mu < 537 \text{ meV}$ or $0.10 < c_{\text{core}} < 0.15$

A strong variation in  $c_3$  and  $c_4$ , as well as in  $c_2$ ,  $c_5$ , and  $c_6$ , can be observed. This leads to a significant change in the concentration profiles (Fig. 6) that exhibit a nonclassical part, i.e., a concave part, spreading over the first four shells. More precisely, the exponential attenuation of the concentration profile is recovered only in the core region, the one close to the surface being subjected to the growth of a Ag-rich phase which is metastable in the bulk. This behavior is typical of a prewetting stage since we observe the existence of a Cu-rich concentration plateau in the core region but not of a Ag-rich one near the cluster surface. We recall that this leads to a complete wetting from the surface in a semi-infinite crystal as  $\Delta\mu \rightarrow \Delta\mu_c^{\text{bulk}}$ .<sup>46,47</sup>

### 3. Stage III: $537 \text{ meV} < \Delta\mu < 542 \text{ meV}$ or $0.15 < c_{\text{core}} < 0.85$

The cluster chemical composition changes drastically from a Ag-rich surface/Cu-rich core state to an almost Ag-

pure state. Note that for an infinite bulk, this stage corresponds to the miscibility gap, in which two states coexist with concentrations equal to the bulk solubility limits at this temperature ( $c_\alpha=0.13$  and  $c_\beta=0.87$ ). As seen in Sec. III, we can wonder whether the first-order phase transition of phase separation of the infinite bulk is replaced with the existence of a dynamical equilibrium of the whole nanoparticle between a Cu-rich state and a Ag-rich one on the corresponding range of  $\Delta\mu$ .

Figure 7(a) shows the variation in the core concentration, the core being defined by the 55 central sites, as a function of the number of MC steps for  $\Delta\mu=539.6$  meV. A dynamical equilibrium is clearly visible, the core concentration oscillating between a Cu-rich state ( $c=0.15$ ) and a Ag-rich state ( $c=0.85$ ). If we look now at the variation in the concentrations for the other internal shells, e.g., shell 5 shown in Fig. 7(b), we can see that a dynamical equilibrium affects also these shells. More precisely, the concentration switches are completely correlated, showing that this is a collective behavior of the whole cluster. The amplitude of the concentration oscillation is even more significant as the shell is close to the core. Like for the cluster surface studied in Sec. III, the core CDOS, shown in Fig. 7(c) (dark gray), is thus bimodal. Moreover, increasing  $\Delta\mu$  leads to a change in the weight of these two states, the Ag-rich state being more populated to the detriment of the Cu-rich one, while the Ag concentrations relative to these two states are almost constant on the whole range of  $\Delta\mu$ . This is similar to a miscibility gap of an infinite bulk, the alloy concentrations inside this domain being a weighted sum of the two solubility limits (the so-called level rule).

The comparison between the evolutions of the core and of the  $S_5$ -shell CDOS [Figs. 7(c) and 7(d)] for the same three values of  $\Delta\mu$  shows an important difference between the behavior of the intermediate shells and the core one. While the Ag concentrations of the two modes are almost constant in the core region, the low-concentration mode for the  $S_5$  shell moves toward highest concentrations as  $\Delta\mu$  increases, the high-concentration mode being almost constant. Since the concentration profile is the weighted sum of a Cu-rich profile and of a Ag-rich one, the concentration of each shell affected by the dynamical equilibrium can be written as

$$c_p(\Delta\mu) = [1 - \alpha(\Delta\mu)]c_p^{\text{low}} + \alpha(\Delta\mu)c_p^{\text{high}}, \quad (1)$$

where  $c_p^{\text{low}}$  and  $c_p^{\text{high}}$  are the  $p$ -shell concentrations of the Cu-rich and Ag-rich states respectively. Using the criterion  $c_{\text{core}} < 0.5$  ( $c_{\text{core}} > 0.5$ ) to define the Cu-rich (Ag-rich) state, one can obtain the evolution of the weight between the two states through the following parameter:

$$\alpha(\Delta\mu) = \frac{N^{\text{conf}}(c_{\text{core}} > 0.5)}{N^{\text{conf}}}, \quad (2)$$

where  $N^{\text{conf}}$  is the total number of configurations of one MC simulation at a given  $\Delta\mu$  and  $N^{\text{conf}}(c_{\text{core}} > 0.5)$  is the number of configurations corresponding to  $c_{\text{core}} > 0.5$  during the same run. Figure 8 shows the resulting concentration profiles and this fully confirms the behavior deduced from the CDOS analysis: the concentration of the Ag-rich state varies very

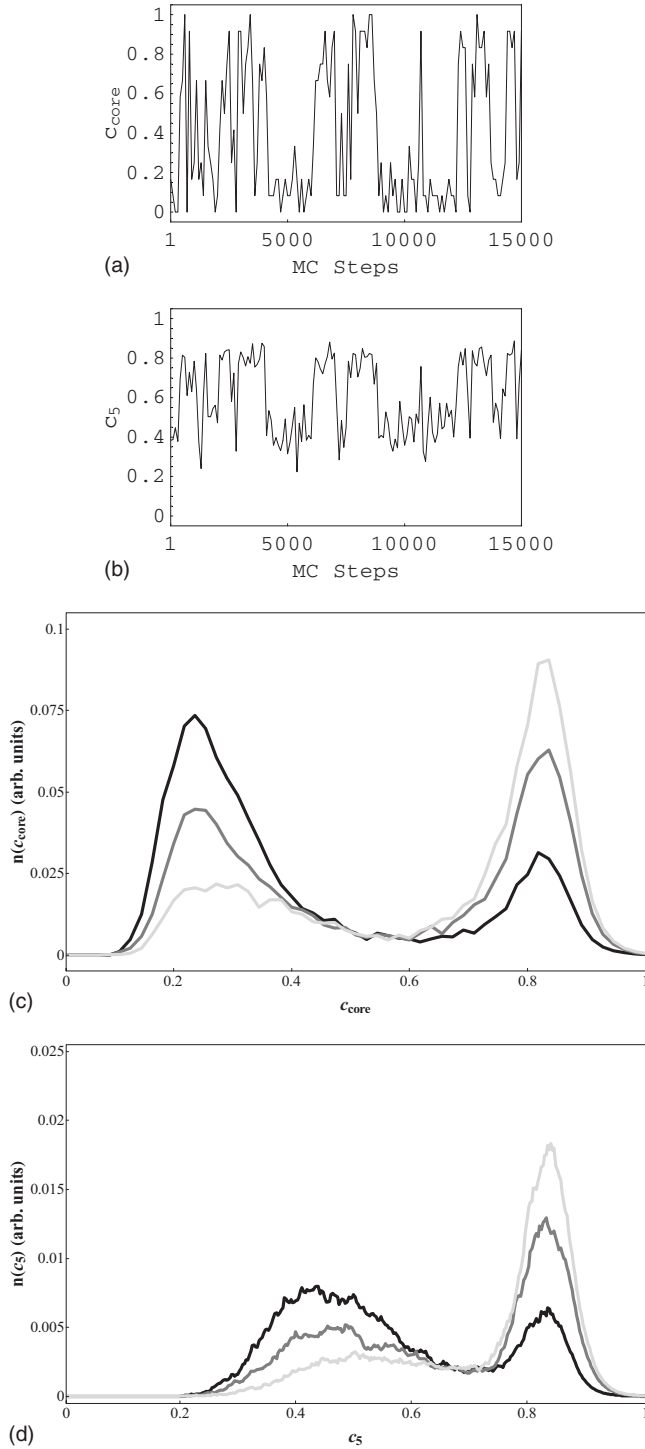


FIG. 7. Variation in the concentration for the core (55 sites from shells  $p=9$  to  $p=11$ ) (a) and for one internal shell ( $p=5$ ) (b) as a function of the number of MC steps for  $\Delta\mu=539.6$  eV at  $T \approx 0.887c_c^{\text{bulk}}$ . CDOSs for the core (55 sites from shells  $p=9$  to  $p=11$ ) (c) and for one internal shell ( $p=5$ ) (d) for various  $\Delta\mu$  lying in stage 3;  $\Delta\mu=539.4$  meV (dark gray),  $\Delta\mu=539.6$  meV (gray), and  $\Delta\mu=539.8$  meV (light gray) at  $T \approx 0.887c_c^{\text{bulk}}$ . Note that for the sake of clarity, we have drawn the line graphs of the histograms.

slightly as a function of  $\Delta\mu$  contrary to the one of the Cu-rich state that is subjected to prewetting, especially for shells 4–8. Therefore, Eq. (1) is still valid as long as the depen-

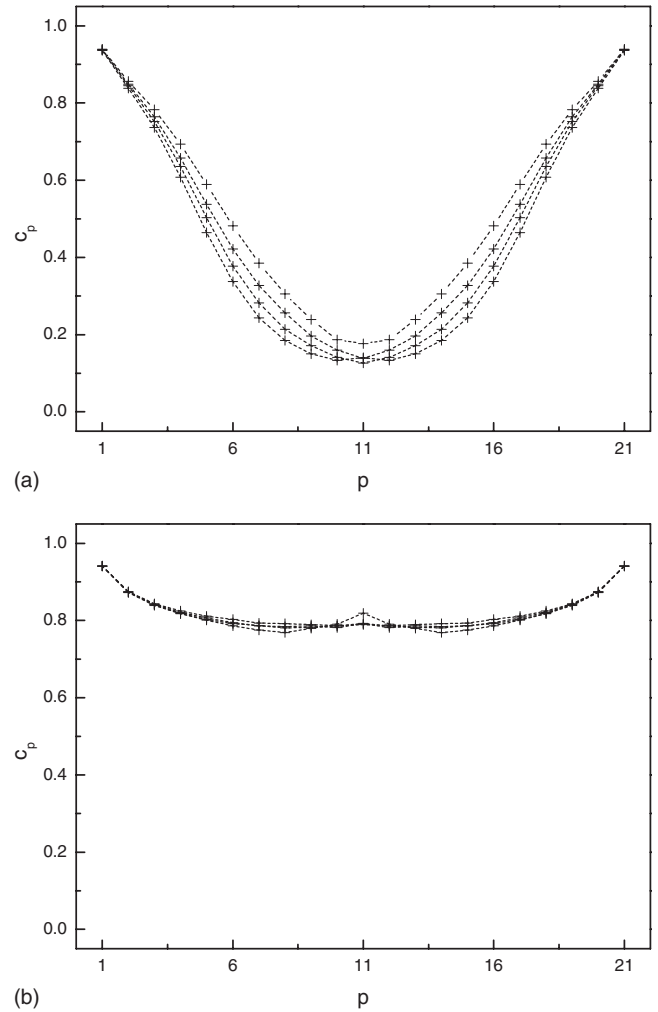


FIG. 8. Concentration profiles,  $c_p=f(p)$ , for the Cu-rich state (a) and for the Ag-rich state (b) for various  $\Delta\mu$  lying in stage 3 at  $T \approx 0.887c_c^{\text{bulk}}$ , from bottom to top:  $\Delta\mu=539.4$  meV,  $\Delta\mu=539.6$  meV,  $\Delta\mu=539.8$  meV, and  $\Delta\mu=540$  meV. For the Ag-rich state, the different profiles are almost identical since this state varies very slightly as a function of  $\Delta\mu$ .

dence of  $c_p^{\text{low}}$  on  $\Delta\mu$  is taken into account, i.e.,  $c_p^{\text{low}} \rightarrow c_p^{\text{low}}(\Delta\mu)$ .

Finally, we can resume the characteristics of stage 3 as follows:

(a) The system oscillates between two states, leading to a bimodal CDOS.

(b) The Ag-rich state varies very slightly as a function of  $\Delta\mu$ , which is expected when referred to the equivalent infinite bulk (a mixing of two phases, each one having a constant concentration over the whole miscibility gap).

(c) On the contrary, the Cu-rich state varies significantly. This is linked to the prewetting behavior of stage 2, which is active for the Cu-rich state in stage 3.

#### 4. Stage IV: $542 \text{ meV} < \Delta\mu$ or $0.85 < c_{\text{core}}$

Similar to stage 1, it is a stage of standard segregation but with a Ag-rich core, the phenomenon being thus much less pronounced than in stage 1. The concentration profiles are again convex (see Fig. 6).

## V. DISCUSSION

One question that arises from this present study is to know how the wetting behavior of the semi-infinite Cu-Ag system is recovered, i.e., the growth from the surface of a wetting film of diverging thickness at the vicinity of the bulk solubility limit,<sup>29,30,46,47</sup> since there is no wetting for the cluster in the present study. Within a mean-field formalism applied to the linear chain, it has been shown that the thickness of the Ag-rich wetting layer formed at each end of the chain for a given  $\Delta\mu$  is<sup>48</sup>

$$e(\Delta\mu) = -\xi \ln(\Delta\mu_c^\infty - \Delta\mu) + C, \quad (3)$$

where  $\xi$  is the attenuation length of the segregation profile and  $\Delta\mu_c^\infty$  is the critical value of  $\Delta\mu$  corresponding to  $c_{\text{bulk}} = 0.5$  for an infinite bulk. The constant  $C$  is equal to  $\xi \ln(B/\xi)$ , where  $B$  is the pre-exponential factor of the repulsive force between the surface and the interface of the wetting phase and the core.<sup>49</sup> For a linear chain made of  $N$  atoms, the maximum thickness of the wetting layer is thus reached when the value of  $\Delta\mu$  corresponds to the existence of the core dynamical equilibrium,  $\Delta\mu_c^N$ , i.e.,  $e_{\text{max}} = e(\Delta\mu_c^N)$ . Therefore, the reliable quantity for enlightening the competition between wetting and core phase transition (or dynamical equilibrium) is  $\delta\Delta\mu_c = \Delta\mu_c^\infty - \Delta\mu_c^N$ . At  $T=0$  K,  $\delta\Delta\mu_c$  is linear with the inverse chain length  $N^{-1}$  but deviates slightly from this linear dependence at finite temperatures.

The nanoparticle core is defined here by the central atom and its 12 nearest neighbors. We have thus calculated  $\delta\Delta\mu_c$  as a function of the cluster size for two temperatures ( $T \approx 0.88T_c^{\text{bulk}}$  and  $T \approx 0.65T_c^{\text{bulk}}$ ). The results are presented in Fig. 9(a) and several comments can be made:

(a)  $\delta\Delta\mu_c$  is positive, leading to  $c_\alpha^{N_{\text{at}}} < c_\alpha^\infty$  and  $c_\beta^{N_{\text{at}}} < c_\beta^\infty$ ,  $c_\alpha^{N_{\text{at}}}$  and  $c_\beta^{N_{\text{at}}}$  being the core solubility limits of a cluster of  $N_{\text{at}}$  atoms.

(b)  $\delta\Delta\mu_c$  decreases rapidly for small values of  $N_{\text{at}}$  ( $N_{\text{at}} < 2000$ ) to tend toward zero with an asymptotic behavior for larger  $N_{\text{at}}$ .

(c)  $\delta\Delta\mu_c$  is even larger as the temperature is low and the cluster size is small.

To take advantage of the linear-chain study, we have checked the variation in  $\delta\Delta\mu_c$  as the inverse of the cluster diameter  $N_{\text{at}}^{-1/3}$ . Due to temperature effects, Fig. 9(b) shows that  $\delta\Delta\mu_c$  is roughly proportional to  $N_{\text{at}}^{-1/3}$  except for the smallest size ( $N_{\text{at}}=55$  atoms), for which the core sites have nearest-neighbor bonds with the surface sites and are thus directly influenced by superficial segregation. However, introducing now  $\Delta\mu_c^\infty - \Delta\mu_c^{N_{\text{at}}} = aN_{\text{at}}^{-1/3}$  [see Fig. 9(b)] into Eq. (3) leads to a qualitative expression of

$$e_{\text{max}} = \frac{\xi}{3} \ln N_{\text{at}}. \quad (4)$$

Equation (4) shows that the thickness of the wetting phase grows very slowly with respect to the nanoparticle size. Indeed, increasing  $N_{\text{at}}$  by a factor of  $10^5$  leads to an increase in  $e_{\text{max}}$  of only three shells. Thus, Eq. (4) allows one to make compatible the prediction of an incomplete wetting for clusters and the observation of a complete wetting for a semi-infinite bulk within the same energetical model.<sup>29,30,50</sup> As

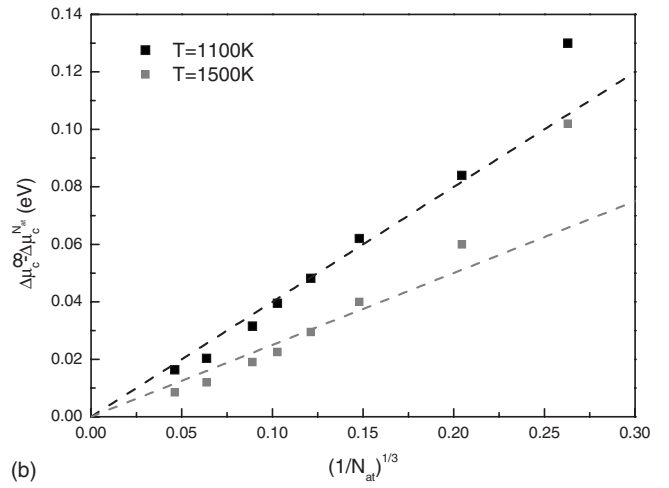
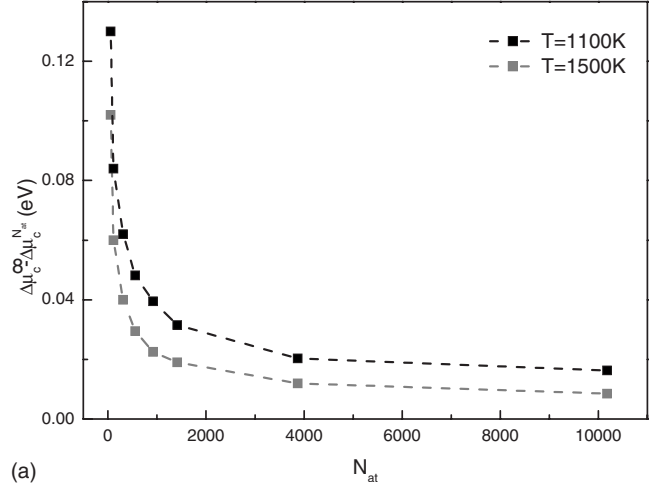


FIG. 9. Dependence of  $\Delta\mu_c^\infty - \Delta\mu_c^{N_{\text{at}}}$  on the cluster size, expressed in number of atoms,  $N_{\text{at}}$ , at  $T \approx 0.65T_c^{\text{bulk}}$  (1100 K) and  $T \approx 0.88T_c^{\text{bulk}}$  (1500 K) (a);  $\Delta\mu_c^\infty - \Delta\mu_c^{N_{\text{at}}}$  as a function of  $N_{\text{at}}^{-1/3}$  at the same temperatures (b). The dashed lines are a guide only for the eyes.

$N_{\text{at}} \rightarrow \infty$ , the thickness of the wetting film tends to infinity but the  $\ln N_{\text{at}}^{-1/3}$  convergence is very slow. Thus, this prevents obtaining a wetting layer of large thickness in clusters made of thousands up to millions of atoms.

## VI. CONCLUSION

In this work, we study the competition between superficial segregation, wetting and core dynamical equilibrium in bimetallic nanoparticles. To resume this point, we present in Fig. 10 diagrams that draw the evolution of the concentration profile as a function of  $\Delta\mu$  at  $T < T_c^{\text{bulk}}$ . Increasing  $\Delta\mu$ , one can distinguish:

(a) Standard segregation, which can be strong if the segregating species is the minor constituent [Fig. 10(a)].

(b) Prewetting, for which the profile exhibits a concave part but without the apparition of a plateau rich in the segregating species [Fig. 10(b)]. For very large clusters, this stage may be followed by partial wetting with the apparition of such a plateau [Fig. 10(b')].

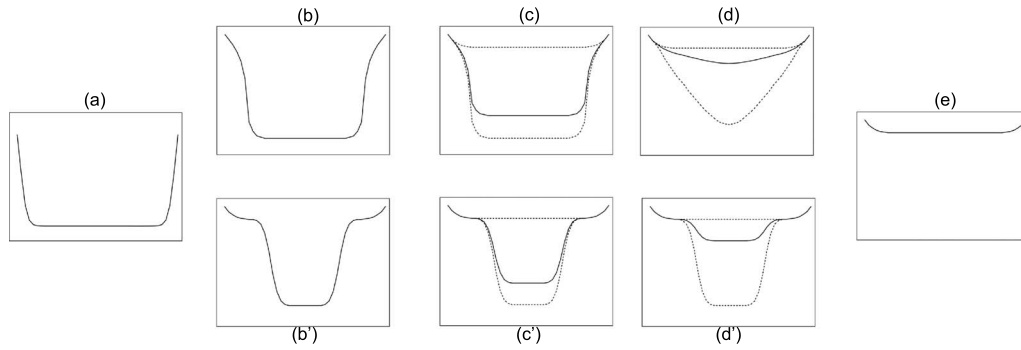


FIG. 10. Schematical evolution of the concentration profile,  $c_p = f(p)$ , as  $\Delta\mu$  increases at  $T < T_c^{\text{bulk}}$  (solid lines), which results from the weighted sum of a Cu-rich profile and a Ag-rich one (dotted lines) [see Eq. (1)]. Standard segregation profile (a), prewetting stage (b) followed by a partial wetting stage for sufficiently large clusters (b'), dynamical equilibrium stage with evolution of the prewetting state for small clusters [(c) and (d)], or without evolution of the partial wetting state for large clusters [(c') and (d')] and again standard segregation profile (e).

(c) Dynamical equilibrium affecting all the internal shells, similar to the first-order phase transition due to the miscibility gap in an infinite crystal. For small clusters, the “solvent”-rich state evolves as a function of  $\Delta\mu$ , while the “solute”-rich one is almost constant [Figs. 10(c) and 10(d)]. For larger clusters, the solvent-rich state corresponds to a partial wetting profile and it is thus reasonable to think that it does not evolve anymore on the dynamical equilibrium range of  $\Delta\mu$  [Figs. 10(c') and 10(d')].

(d) Standard segregation but weak, since the segregating species is the major constituent [Fig. 10(e)].

Moreover, during the first stage of standard segregation, a similar behavior can be observed for the cluster facets if the temperature is lower than the critical temperatures of the corresponding surfaces of semi-infinite crystals. Finally, recall that the Wulff polyhedron is generally more stable than the cuboctahedron. If details of the segregation behaviors may differ between the two structures, the dynamical equilibrium of the core as well as the competition between wetting and dynamical equilibrium do not, since both structures are constructed on the fcc lattice.

It is worthy to note that this summary is obtained from Monte Carlo simulations in the pseudo-grand-canonical ensemble, in which the number of atoms of each species is given by the difference in chemical potentials of the constituents,  $\Delta\mu$ , the total number of atoms being fixed. From an experimental point of view, it is more usual to characterize a nanoparticle assemblage of the narrowest size distribution as possible with a fixed mean nominal concentration. The dynamical equilibrium observed in our simulations may thus manifest itself as:

(a) A dynamical equilibrium in each cluster, but it would require a huge transport of matter with the reservoir (vapor or deposited atoms on a substrate) to allow such concentration variations for each cluster. Yet, it seems not likely that such transport of matter can occur, mainly due to kinetic limitations.

(b) The apparition of two types of nanoparticles, one corresponding to clusters in the solute-rich state, the other cor-

responding to clusters in the solvent-rich state, the ratio of the two types of nanoparticles depending on the reservoir with which these nanoparticles are in equilibrium.

Actually, this second point, already mentioned in Ref. 17, seems to be observed in recent experimental studies on Cu-Ag clusters<sup>51</sup> but still has to be completed with studies about shape and size effects.

On the other hand, the question about the equilibrium of an isolated nanoparticle of fixed nominal concentration within the domain of dynamical equilibrium is still open. For the cluster surface, the dynamical equilibrium affects each facet separately, which means that each facet behaves with each other as a reservoir. Therefore, experimental evidence of the dynamical equilibrium consequences should be possible, i.e., mixing between solute-rich and solvent-rich facets of the same crystallographical type. On the contrary, for the whole nanoparticle, one may think that the solute-rich superficial phase will grow toward the cluster core, leading to a wetting-type concentration profile. However, the study within the pseudo-grand-canonical ensemble shows that it is not wetting from a thermodynamical point of view but is rather a coexistence of two phases, even if the aspect of the concentration profile cannot differentiate between these two situations. Simulations in the canonical ensemble, in which both the number of atoms and the nominal concentration are fixed, should bring further information to answer this question.

This study can thus be considered as a significant step in the building of phase diagrams for bimetallic nanoparticles. Works are in progress to go beyond the rigid-lattice approximation in order to account for relaxation effects due to the size difference between the two constituents on one hand and to study the effect of strain/stress of the facets during the segregation stage for noncrystallographic structures, e.g., icosahedron, on the other hand.

#### ACKNOWLEDGMENTS

It is a great pleasure to thank R. Tétot, C. Mottet, and G. Trégliat for fruitful discussions.

\*Corresponding author; jerome.creuze@u-psud.fr

- <sup>1</sup>R. Ferrando, J. Jellinek, and R. L. Johnston, *Chem. Rev. (Washington, D.C.)* **108**, 845 (2008).
- <sup>2</sup>S. Sao-Joao, S. Giorgio, J. M. Penisson, C. Chapon, S. Bourgeois, and C. Henry, *J. Phys. Chem. B* **109**, 342 (2005).
- <sup>3</sup>B. Skarman, T. Nakayama, D. Grandjean, R. E. Benfield, E. Olsson, K. Niihara, and L. R. Wallenberg, *Chem. Mater.* **14**, 3686 (2002).
- <sup>4</sup>N. Toshima, *Pure Appl. Chem.* **72**, 317 (2000).
- <sup>5</sup>N. Toshima, M. Harada, Y. Yamazaki, and K. Asakura, *J. Phys. Chem.* **96**, 9927 (1992).
- <sup>6</sup>L. Favre, S. Stanesco, V. Dupuis, E. Bernstein, T. Epicier, P. Melinon, and A. Perez, *Appl. Surf. Sci.* **226**, 265 (2004).
- <sup>7</sup>H. Zeng, J. Li, Z. L. Wang, J. P. Liu, and S. Sun, *Nano Lett.* **4**, 187 (2004).
- <sup>8</sup>S. Basu and D. Chakravorty, *J. Non-Cryst. Solids* **352**, 380 (2006).
- <sup>9</sup>M. Gaudry, E. Cottancin, M. Pellarin, J. Lermé, L. Arnaud, J. R. Huntzinger, J. L. Vialle, M. Broyer, J. L. Rousset, M. Treilleux, and P. Mélinon, *Phys. Rev. B* **67**, 155409 (2003).
- <sup>10</sup>J. Zhu, Y. Wang, L. Huang, and Y. Lu, *Phys. Lett. A* **323**, 455 (2004).
- <sup>11</sup>F. Ducastelle, *Order and Phase Stability in Alloys* (North-Holland, Amsterdam, 1991).
- <sup>12</sup>G. Tréglia, B. Legrand, F. Ducastelle, A. Saúl, C. Gallis, I. Meunier, C. Mottet, and A. Senhaji, *Comput. Mater. Sci.* **15**, 196 (1999).
- <sup>13</sup>F. Lequien, J. Creuze, F. Berthier, and B. Legrand, *J. Chem. Phys.* **125**, 094707 (2006).
- <sup>14</sup>V. Moreno, J. Creuze, F. Berthier, C. Mottet, G. Tréglia, and B. Legrand, *Surf. Sci.* **600**, 5011 (2006).
- <sup>15</sup>L. Rubinovich and M. Polak, *Phys. Rev. B* **69**, 155405 (2004).
- <sup>16</sup>M. Polak and L. Rubinovich, *Int. J. Nanosci.* **3**, 625 (2004).
- <sup>17</sup>M. Polak and L. Rubinovich, *Phys. Rev. B* **71**, 125426 (2005).
- <sup>18</sup>G. Wang, M. A. Van Hove, P. N. Ross, and M. I. Baskes, *J. Chem. Phys.* **121**, 5410 (2004).
- <sup>19</sup>G. Wang, M. A. Van Hove, P. N. Ross, and M. I. Baskes, *J. Chem. Phys.* **122**, 024706 (2005).
- <sup>20</sup>R. L. Johnston, *Atomic and Molecular Clusters* (Taylor & Francis, London, 2002).
- <sup>21</sup>J. Jellinek and E. B. Krissinel, *Theory of Atomic and Molecular Clusters* (Springer, Berlin, 1999), p. 277.
- <sup>22</sup>R. H. Fowler and E. H. Guggenheim, *Statistical Thermodynamics* (Cambridge University Press, Cambridge, England, 1960).
- <sup>23</sup>Y. Liu and P. Wynblatt, *Surf. Sci.* **241**, L21 (1991).
- <sup>24</sup>J. Eugène, B. Aufray, and F. Cabané, *Surf. Sci.* **241**, 1 (1991).
- <sup>25</sup>R. Tétot, F. Berthier, J. Creuze, I. Meunier, G. Tréglia, and B. Legrand, *Phys. Rev. Lett.* **91**, 176103 (2003).
- <sup>26</sup>I. Braems, F. Berthier, J. Creuze, R. Tétot, and B. Legrand, *Phys. Rev. B* **74**, 113406 (2006).
- <sup>27</sup>F. Berthier, J. Creuze, R. Tétot, and B. Legrand, *Phys. Rev. B* **65**, 195413 (2002).
- <sup>28</sup>See, for example, S. Dietrich, in *Phase Transitions and Critical Phenomena*, edited by C. Domb and J. L. Lebowitz (Academic, London, 1988), Vol. 12, p. 1.
- <sup>29</sup>Y. Teraoka and T. Seto, *Surf. Sci.* **255**, 209 (1991).
- <sup>30</sup>A. Saúl, B. Legrand, and G. Tréglia, *Surf. Sci.* **331-333**, 805 (1995).
- <sup>31</sup>F. L. Williams and D. Nason, *Surf. Sci.* **45**, 377 (1974).
- <sup>32</sup>M. E. Fisher, *Rep. Prog. Phys.* **30**, 615 (1967).
- <sup>33</sup>F. Berthier, B. Legrand, and G. Tréglia, *Acta Mater.* **47**, 2705 (1999).
- <sup>34</sup>J. Creuze, F. Berthier, R. Tétot, and B. Legrand, *Phys. Rev. B* **62**, 2813 (2000).
- <sup>35</sup>I. Braems, J. Creuze, F. Berthier, R. Tétot, and B. Legrand, *Surf. Sci.* **602**, 1903 (2008).
- <sup>36</sup>F. Baletto, R. Ferrando, A. Fortunelli, F. Montalenti, and C. Mottet, *J. Chem. Phys.* **116**, 3856 (2002).
- <sup>37</sup>C. Mottet, J. Goniakowski, F. Baletto, R. Ferrando, and G. Tréglia, *Phase Transitions* **77**, 101 (2004).
- <sup>38</sup>S. M. Foiles, *Phys. Rev. B* **32**, 7685 (1985).
- <sup>39</sup>K. Binder, *The Monte Carlo Method in Condensed Matter Physics* (Springer-Verlag, Berlin, 1995).
- <sup>40</sup>N. Metropolis, A. W. Metropolis, M. N. Rosenbluth, A. H. Teller, and E. Teller, *J. Chem. Phys.* **21**, 1087 (1953).
- <sup>41</sup>K. Binder and D. P. Landau, *Phys. Rev. B* **30**, 1477 (1984).
- <sup>42</sup>M. Hansen and K. Anderko, *Constitution of Binary Alloys* (McGraw-Hill, New York, 1958).
- <sup>43</sup>C. Mottet, G. Rossi, F. Baletto, and R. Ferrando, *Phys. Rev. Lett.* **95**, 035501 (2005).
- <sup>44</sup>J. Tersoff, *Phys. Rev. B* **42**, 10965 (1990).
- <sup>45</sup>M. Cazayous, C. Langlois, T. Oikawa, C. Ricolleau, and A. Sacuto, *Phys. Rev. B* **73**, 113402 (2006).
- <sup>46</sup>R. Pandit and M. Wortis, *Phys. Rev. B* **25**, 3226 (1982).
- <sup>47</sup>R. Pandit, M. Schick, and M. Wortis, *Phys. Rev. B* **26**, 5112 (1982).
- <sup>48</sup>F. Lequien, J. Creuze, F. Berthier, and B. Legrand, *Faraday Discuss.* **138**, 105 (2008).
- <sup>49</sup>F. Lequien, J. Creuze, F. Berthier, and B. Legrand (unpublished).
- <sup>50</sup>R. Lipowsky, *Critical Phenomena at Surfaces and Interfaces*, Springer Tracts in Modern Physics Vol. 127 (Springer-Verlag, Berlin, 1993).
- <sup>51</sup>C. Langlois, D. Alloyeau, Y. Le Bouar, A. Loiseau, T. Oikawa, C. Mottet, and C. Ricolleau, *Faraday Discuss.* **138**, 375 (2008).